Trap-Induced Losses in Hybrid Photovoltaics

Feng Gao,[†] Zhe Li, Jianpu Wang, Akshay Rao, Ian A. Howard, Agnese Abrusci, Sylvain Massip, Christopher R. McNeill,[‡] and Neil C. Greenham*

Cavendish Laboratory, University of Cambridge, J J Thomson Avenue, Cambridge CB3 0HE, United Kingdom. [†]Present address: Biomolecular and Organic Electronics, IFM, and Center of Organic Electronics, Linköping University, SE-581 83 Linköping, Sweden. [‡]Present address: Department of Materials Engineering, Monash University, Wellington Road, Clayton, Victoria, 3800 Australia.

ABSTRACT We investigate the loss mechanisms in hybrid photovoltaics based on blends of poly(3-hexylthiophene) with CdSe nanocrystals of various sizes. By combining the spectroscopic and electrical measurements on working devices as well as films, we identify that high trap-mediated recombination is responsible for the loss of photogenerated charge carriers in devices with small nanocrystals. In addition, we demonstrate that the reduced open-circuit voltage for devices with small nanocrystals is also caused by the traps.

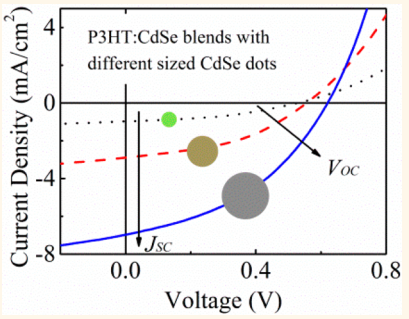

KEYWORDS: hybrid solar cells · trap · charge transport and recombination · transient absorption · transient photocurrent · CdSe nanocrystals

Semiconducting nanocrystals (NCs) are an attractive candidate as the acceptor material in bulk heterojunction (BHJ) organic photovoltaics (OPVs) due to their high dielectric constant, tunable energy levels, and ability to form controlled nanostructures. Although the efficiency of the first hybrid OPV device was very low,[1] shape engineering for NCs in the past decade has provided breakthroughs in hybrid OPV research.[2−4] In addition to shape engineering, another focus for hybrid OPV research lies in the interface between the polymeric donor and the nanocrystalline acceptor.[5] By treating the polymer:nanocrystal hybrid film in an ethanedithiol-containing acetonitrile solution, Ren *et al.* achieved an efficiency of more than 4%, demonstrating further promise for hybrid OPVs.[6]

However, considering the potential advantages of NCs, the efficiency achieved so far is still far from what might be expected, and the reason for this discrepancy remains poorly understood. In order to further improve device performance, the loss processes limiting device performance need to be discerned. Dayal *et al.* performed electrodeless flash photolysis time-resolved microwave conductivity measurements on poly(3-hexylthiophene) (P3HT):CdSe devices with different CdSe nanoparticle shapes.[7] They found that the charge lifetime increased as the shape became more complex. Accordingly, they suggested that nanorods and tetrapods provide an easier pathway for electrons to move away from the dissociation site, hence enhancing the free carrier generation. However, with the change in shape, various other parameters might have been significantly changed, which complicates the analysis of this type of data.

In this paper, we present investigations of P3HT:CdSe devices with different sized CdSe nanodots. By varying the nanoparticle size but keeping nanoparticle shape constant, we are able to focus on the influence of interfacial area and electron confinement. On the basis of the results of steady-state and transient measurements, we propose that the traps associated with CdSe NC surfaces play a key role in controlling device performance.

RESULTS AND DISCUSSION

The synthesis of different sized NCs and the fabrication of PV devices are described in the Methods section. The three different

* Address correspondence to ncg11@cam.ac.uk.

Received for review March 18, 2013 and accepted March 7, 2014.

Published online March 07, 2014
10.1021/nn501185h

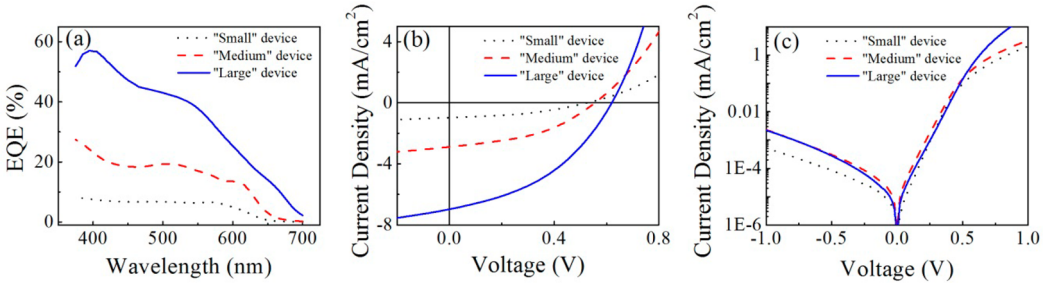

Figure 1. Steady-state characteristics of P3HT:CdSe devices with different NC sizes. (a) EQE; (b) *J*−*V* curves under the solar simulator (illumination intensity equivalent to 100 mW/cm^2 AM1.5G conditions after spectral mismatch correction); (c) dark *J*−*V* curves.

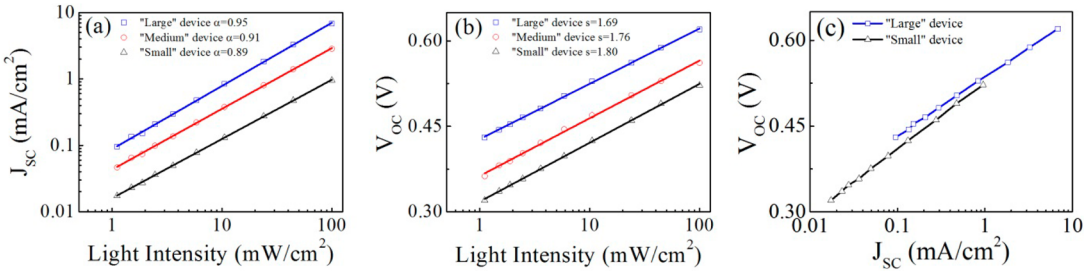

Figure 2. Light-intensity dependence of (a) short-circuit current and (b) open-circuit voltage. The points are the raw data. The solid lines in (a) are fits to the expression of $J_{SC} \propto I^{\alpha}$, while those in (b) are fits to the expression of $V_{OC} = s(kT/q)\ln(I) + \text{constant}$. *I* is the incident light intensity, and *kT*/*q* at room temperature is 0.025 V. (c) V_{OC} *versus* J_{SC} at different intensities for the large and small devices.

sized NCs have average diameters of 3.3, 4.4, and 5.3 nm, as revealed by both TEM images and empirical calculations based on the first absorption peak.[8] In the following text, the P3HT:CdSe devices blended with these three sized nanodots are denoted as "small", "medium", and "large" devices, respectively.

Figure 1 presents the steady-state photovoltaic characteristics of the P3HT:CdSe devices with three different NC sizes. As shown in Figure 1a, with increasing size, the external quantum efficiency (EQE) value demonstrates a significant increase. Consistent with the striking increase in the EQE, J_{SC} under the solar simulator (100 mW/cm^2 AM1.5G) also shows pronounced improvement with increasing size. As shown in Figure 1b, J_{SC} increases by almost a factor of 6 from the small device (0.97 mA/cm^2) to the large device (6.97 mA/cm^2). Another parameter, V_{OC}, also increases as the size increases. V_{OC} is usually believed to be determined by the difference between the donor highest occupied molecular orbital (HOMO) and the acceptor lowest unoccupied molecular orbital (LUMO). With increasing size, the CdSe LUMO moves closer to the P3HT HOMO. Therefore, V_{OC} is expected to decrease as the size increases, which is in contrast to our experimental results. We consider the possibility that the dark current affects V_{OC}, due to different shunt pathways in devices with different sized NCs. Subtracting the dark current (Figure 1c) from the current under simulated solar illumination, the resulting voltage, V_0, at which photocurrent is zero can be determined. V_0 also increases with increasing size, which excludes the effect of the dark current.

We also performed light-intensity-dependent measurements of J_{SC} and V_{OC}. As shown in Figure 2a, J_{SC} for all three devices increases sublinearly with the light intensity (*I*). The value of α, the fitting coefficient to the power law fit $J_{SC} \propto I^{\alpha}$, increases from 0.89 for the small device to 0.95 for the large device. This means that light-intensity-dependent processes, that is, bimolecular recombination and/or space-charge effects, are not significant at short-circuit conditions, especially for the large device. In addition, the fact that the difference in α between different devices is not striking indicates that the light-intensity-dependent loss processes are unlikely to be the primary reasons for the 600% increase in short-circuit current with increasing NC size.

The open-circuit voltages of the devices scale logarithmically with the light intensity, resulting in straight lines in the semilog plot of Figure 2b. It has been demonstrated that V_{OC} can be written as[9,10]

$$V_{OC} = \frac{E_{gap}}{q} - \frac{kT}{q}\ln\left(\frac{N_c^2}{np}\right) \quad (1)$$

where E_{gap} is the effective energy band gap of the blend, *q* is the elementary charge, *k* is Boltzmann's constant, *T* is the temperature, *n* (*p*) is the electron (hole) density, and N_c is the effective density of states. Since all the charges recombine at V_{OC}, the generation rate of polaron pairs *G* is equal to the recombination rate *R*. Depending on whether the recombination is

first-order (geminate recombination or trap-assisted recombination) or second-order (bimolecular recombination), R is proportional to $(np)^{1/2}$ or np. This means that G is proportional to $(np)^{1/2}$ in the first-order recombination case and np in the second-order recombination case. Since G scales linearly with the light intensity, eq 1 predicts the slope of skT/q of V_{OC} scaling with ln(I), with $s = 1$ when second-order recombination dominates and $s = 2$ when first-order recombination dominates. All the s values in our fitting lie between 1 and 2, which indicates that the first- and second-order recombination coexist in the devices at V_{OC}. We suggest that the first-order recombination is due to trap-mediated recombination, which is consistent with subsequent transient measurements.

We have mentioned that the increase of V_{OC} with increasing NC size is in contrast to what we expect from the difference between the donor HOMO and acceptor LUMO. Based on the diode equation, the V_{OC} increase could potentially be explained from the rise in J_{SC}. We therefore plot V_{OC} *versus* J_{SC} for the small and large devices at different light intensities in Figure 2c. However, as we can see in Figure 2c, V_{OC} of the large device is always larger than that of the small device at the same J_{SC}. This means that the increase of V_{OC} with NC increasing could not be explained by the diode equation, particularly since the diode saturation current (Figure 1c) is greater in the large device, which would lead to a decrease in V_{OC} within the diode model. Thus the V_{OC} clearly increases with nanoparticle size (by a large amount at constant intensity and a smaller amount at constant current), in contrast to the decrease that would be expected from a simple consideration of the LUMO energy level. The reasons for this are discussed further below.

In order to further understand the origin of the significant difference in device performance, we proceed to investigate the processes from light absorption to charge extraction. Based on absorption measurements, from the small device to the large device, the increase in photon absorption is less than 15%, which is negligible compared with 600% increase in photocurrent generation. Thus the differences in device performance are the result of subsequent processes which are investigated below.

Transient absorption (TA) measurements, especially photoinduced absorption decay kinetics, provide direct information on the evolution of excited-state populations after excitation.[11−13] TA measurements have been widely used to study the dynamics of charge generation and recombination in bulk heterojunction systems.[14−17] Recently, it has become possible to perform these measurements on working devices, allowing the effect of the internal electric field to be investigated.[18−20] In general, pump−probe TA measurements can study processes occurring on time scales from femtoseconds to microseconds, although it

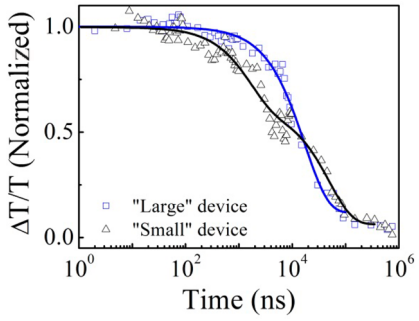

Figure 3. Normalized TA kinetics for large and small P3HT:CdSe devices measured under short-circuit conditions. Charge kinetics were integrated over 875−975 nm. The intensity of the 532 nm excitation pulse was 2 μJ/cm^2. The solid lines are guides for the eye.

is important to work at excitation densities comparable to those in working devices in order for the physics not to be dominated by bimolecular processes. The early time TA of polymer:nanoparticle blends is complex, due to the overlap of features from bleaching, stimulated emission, and induced absorption in the polymers and the nanoparticles. Here, we concentrate on times >1 ns, probing around 900 nm where an induced absorption is seen that can straightforwardly be attributed to the presence of holes (polarons) on the polymer.[20−22]

Figure 3 compares the TA kinetics between the large and small devices under short-circuit conditions. The TA signal is almost flat for the first 100 ns for the small device, while the flat region extends to 1 μs for the large device. Geminate recombination in BHJ systems is usually believed to play its role within 100 ns, beyond which the decay is due to recombination of separated charges as well as charge extraction.[23] The faster signal decay after 100 ns for the small device is unlikely to result from more rapid charge extraction, considering its much smaller photocurrent compared with the large device. Instead, it results from some long-time scale recombination, such as bimolecular recombination or trap-mediated recombination. Since the significant difference in short-circuit current appears even at low intensity (as revealed by the EQE and light-intensity-dependent J_{SC} measurements), the difference is unlikely to result from light-intensity-dependent processes such as pure bimolecular recombination or from electric field redistribution due to space-charge effects. Therefore, we propose that the faster decay for the small device is due to stronger trap-mediated recombination, which will be further confirmed by transient photocurrent measurements. For the large device, if we assume that the signal decay is attributed to charge extraction, the first 10% of charges are collected within 1.1 μs, corresponding to a mobility of 4×10^{-9} m^2 V^{-1} s^{-1}. This value is almost 2 orders of magnitude smaller than that in annealed P3HT:PCBM devices.[20] This indicates that it is likely that there are trapping

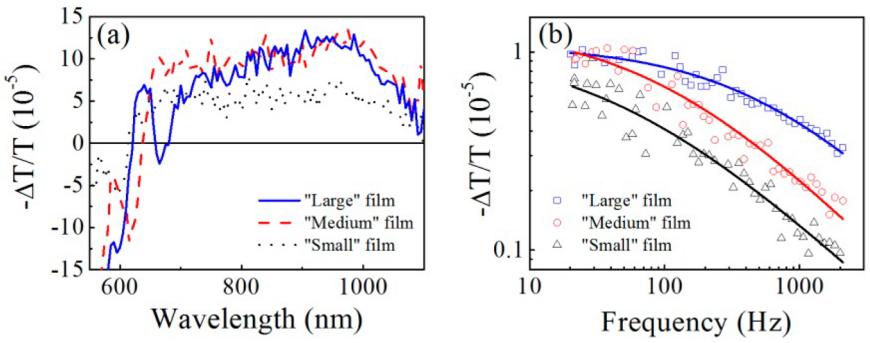

Figure 4. (a) PIA spectra of the blend films with different sized NCs at room temperature. The excitation modulation frequency is 225 Hz. (b) Frequency dependence of the PIA signal at 950 nm for the three films. The points are the raw data, while the solid lines are the fitted curves (see text for the fitting equation). For all the measurements, the excitation laser wavelength is 515 nm, with the intensity of 25 mW/cm^2.

TABLE 1. Fitting Parameters for Frequency-Dependent PIA Signals of the Blend Films with Different Sized NCs

parameters	small film	medium film	large film
τ (ms)	21	10	1.8
γ	0.64	0.69	0.71

effects even in the large device, resulting in slow charge extraction.

Further information on the long-time scale recombination is revealed by photoinduced absorption (PIA) measurements. PIA is a quasi-steady-state pump–probe technique, which is useful to detect long-lived (>10 μs) excited states, such as polarons or triplet excitons. In addition, if the lifetimes of the excited species exceed the inverse of excitation frequency, their absorption will be suppressed in the PIA signal. Therefore, we can obtain the information on lifetime distribution and recombination dynamics of these charge carriers by varying the excitation frequency.

The PIA spectra of the blend films with different sized NCs are shown in Figure 4a. For pure P3HT, no PIA signal is observed (not shown) at room temperature. However, for all three blend films, a broad photoinduced absorption centered at 950 nm is present, indicating the generation of long-lived excited states. Figure 4b shows the frequency dependence of the PIA signals at 950 nm for the three films. For monomolecular or bimolecular recombination dynamics, the PIA signal is expected to saturate at low frequency.[24] However, the PIA signals for the P3HT:CdSe blend films decrease steadily with increasing frequency in the investigated range and cannot be fitted using monomolecular or bimolecular recombination dynamics. To account for trapping effects, a model for dispersive recombination was proposed[25]

$$-\frac{\Delta T}{T} = \frac{(\Delta T/T)_0}{1+(\omega\tau)^\gamma} \qquad (2)$$

where $(\Delta T/T)_0$ is the PIA signal at $\omega = 0$, ω is the excitation modulation frequency, τ is the mean lifetime of the excited species, and γ (<1) is the dispersion

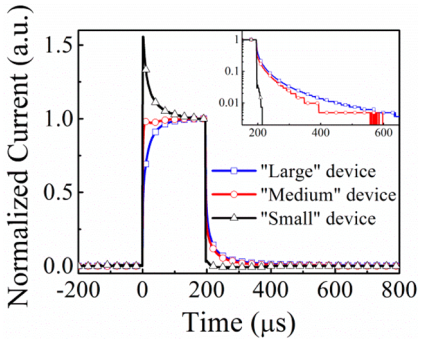

Figure 5. Normalized transient short-circuit photocurrent for three P3HT:CdSe devices in response to 200 μs square-pulse illumination (pulse wavelength 525 nm) at 23 mW/cm^2. The inset highlights the decay dynamics.

constant. As shown in Figure 4b, this equation fits the frequency dependence of PIA signals very well, with the fitted values summarized in Table 1.

The fact that dispersive recombination taking into account trapping effects can fit the experimental data well means that there is a significant amount of traps in all three blends. With decreasing NC size, the dispersion constant decreases, suggesting that the relaxation dynamics become increasingly dispersive and that trapping effects become increasingly significant. The lifetime extending to the millisecond regime is quite long. Indeed, similar lifetime values have been reported in other polymer:CdSe blends.[26,27] When trapping effects in the films are considered, the excited species being probed here are likely to be the trapped carriers, consistent with long lifetimes. The films with smaller NCs show longer lifetimes, which might suggest more severe trapping effects in blend films with smaller NCs. This is consistent with the increasing dispersion with decreasing NC size, as revealed by the decreasing dispersion constant.

In order to further examine the role of traps, we have performed transient photocurrent measurements on the three devices. By investigating how the photocurrent responds to pulsed illumination, transient

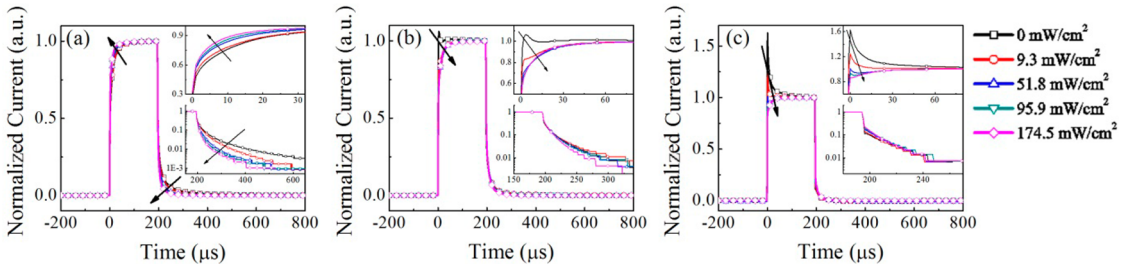

Figure 6. Normalized background-dependent transient photocurrent dynamics for (a) large, (b) medium, and (c) small P3HT:CdSe devices. The measurement was performed under short-circuit conditions. The background light was provided by a white high-brightness LED, and the square-pulse illumination (27 mW/cm^2) was provided by a high-brightness 525 nm green LED. The insets highlight the rise and decay dynamics. The arrow indicates the direction of increasing background intensity.

photocurrent measurements provide direct information on charge transport, recombination, and trapping.[28,29]

Figure 5 shows the normalized transient short-circuit photocurrent of the three P3HT:CdSe devices, in response to 200 μs square-pulse illumination (525 nm) at 23 mW/cm^2. There is an obvious difference between the rise dynamics of different devices. For the large device, a very fast rise in the first 3 μs is followed by a slow rise to the steady-state current. For the small device, the fast initial rise leads to an overshoot of more than 150% of the steady-state current. Such behavior has been observed in polymer/polymer devices[30] and attributed with the aid of numerical modeling[31] to trapping and detrapping effects. Specifically, the overshoot results from the time taken for the trap population to reach equilibrium, which is significantly slower than the time taken for free charges to exit the device. The recombination rate of trap-mediated recombination increases as the trap population increases before settling to a steady-state value when the trap population equilibrates. Based on this modeling work, the large overshoot in the rise dynamics indicates significant trap-mediated recombination in the small device. The medium device shows behavior between that of the large and small devices. After the initial quick rise, a small overshoot is observed, especially for low pulse intensities (not shown). This is again an indication of trap-mediated recombination, although much less pronounced compared with the small device. Therefore, by comparing the rise dynamics of different devices, we can conclude that trap-mediated recombination is becoming stronger with decreasing NC size, which is consistent with the fact that photocurrent generation decreases with decreasing NC size.

The photocurrent decay time at turn-off also shows differences between different devices, with "smaller" devices demonstrating shorter decay time. For the large device, after the initial quick extraction of free carriers within tens of microseconds, there is a long photocurrent tail, with charges continuing to be extracted more than 400 μs after turning off the illumination. As a comparison, in P3HT:PCBM devices, almost all of the carriers are extracted within 50 μs.[28] The long extraction time suggests that a slow detrapping process is involved, which is consistent with our suggestion based on transient absorption measurements that there are also trapping effects in the large device. For the small device, considering its significant trap-mediated recombination, it is unlikely that the very short decay time is due to efficient carrier extraction. Instead, it is caused by the significant number of deep traps, from which carriers do not escape, instead finally recombining with holes.

Further insight into this argument is provided by quantifying the amount of charge extracted after turning off the light. The extracted charge is calculated by integrating the photocurrent with respect to time. In the presence of recombination, this integrated extracted photocurrent sets a lower limit on the number of charges present in the device prior to turn-off. There is almost 2 orders of magnitude difference in extracted charge between the large and small devices at an intensity of 47 mW/cm^2 (short-circuit conditions), with 3.6×10^{-9} C extracted for the former and 4.7×10^{-11} C for the latter. This striking difference agrees with our assertion that in the small device there is a significant number of deeply trapped electrons that cannot be extracted, which finally recombine. Therefore, the fact that both the decay time and the amount of extracted charge increase with increasing size suggests that the detrapping is easier for the large device.

Based on the above analysis, there are traps in all three devices, with charge trapping affecting the device performance even for the large device. The detrapping is less efficient for smaller devices, which contributes to more recombination loss in the smaller devices, consistent with steady-state photocurrent measurements. In order to investigate whether the density as well as the depth of trap states increases with decreasing size, we have also performed transient photocurrent measurements with a constant background light superimposed on the pulsed illumination.

Figure 6 shows the normalized short-circuit photocurrent response to 200 μs square-pulse illumination (525 nm, 27 mW/cm^2) as a function of background light intensity (white light) for the three P3HT:CdSe devices. For the large device (Figure 6a), the rise/decay

dynamics quicken with the background light imposed. This is attributed to the filling of trap sites by the charges generated by the background light, which makes the charge transport easier. When the background light increases above about 50 mW/cm^2, the quickening in the rise/decay dynamics becomes less prominent. This indicates that the traps are almost fully filled with about 50 mW/cm^2 background light. The minor quickening above this intensity may be attributed to carrier-density-dependent mobility.[32] Indeed, if we fix the background light intensity at 52 mW/cm^2 and change the pulse intensity, the normalized traces lie almost on top of each other (not shown). This further confirms that the traps are almost fully filled at this background intensity.

For the medium device (Figure 6b), the imposition of background light eliminates the overshoot after the turn-on with the rise dynamics becoming independent of the background light intensity over 50 mW/cm^2. The disappearance of the overshoot with increasing background illumination intensity similarly results from a filling of the trap states and the pulse of illumination no longer representing a significant perturbation to charge the density in the device. For the small device (Figure 6c), in contrast, the overshoot after the turn-on is still observable for the highest background intensity investigated. This observation indicates that even at high background illumination there is still a significant number of unoccupied trap sites.

The above experiments indicate that it becomes increasingly difficult for the traps to be fully filled for smaller NC sizes. We suggest that the difficulty in filling up the traps in the smaller devices is a consequence of an increasing density of trap states with decreasing NC size, along with an increased recombination rate of trapped charges. This argument is qualitatively reasonable if we assume that the traps are energetic in nature and associated with the NC surface,[33−35] with increasing surface-to-volume ratio as the size decreases. In addition, this argument is further backed up by the possibility of CdSe NCs serving as morphological traps. For the small NCs, there can be poor interconnectivity between dots, meaning that individual NCs can serve as traps.

Further information on recombination dynamics is provided by transient photovoltage (TPV) measurements. We have found that the photovoltage decay kinetics in P3HT:CdSe blends are not well-described by a single-exponential decay.[28] Instead, they could only be fitted with triexponential fits. Following the paper by O'Regan *et al.*,[36] we performed V_{OC}-dependent TPV measurements on large and small devices. As shown in Figure 7, although there are three recombination rate constants for each device, all of the recombination constants are exponentially dependent on V_{OC}, with the same slope in the semilog plot of 10.4 ± 0.2 decades/V. This indicates that the underlying recombination

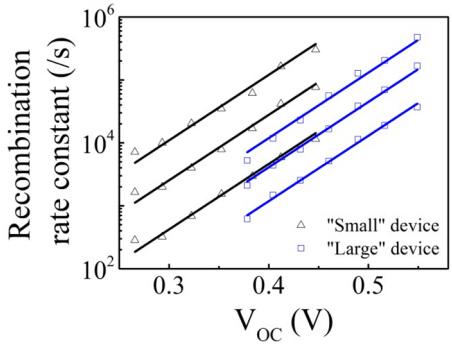

Figure 7. Recombination rate constant *versus* V_{OC} for the large and small devices. The photovoltage decay kinetics in P3HT:CdSe blends can only be fitted with triexponential fits, which result in three recombination constants at each V_{OC}. The solid lines are guides for the eye with a slope of 10.4 ± 0.2 decades/V.

mechanisms are the same for the three decay channels in each device as well as for these two different devices.[36] We attribute this underlying recombination mechanism to trap-assisted recombination. This is consistent with other spectroscopic and electrical evidence in the paper as well as our core concept; that is, trap states limit the performance in hybrid OPVs. Ideally, we would also calculate the capacitance and density of trap states at each V_{OC} using the transient photovoltage data. However, it turned out to be difficult in our case, limited by the difficulty in integrating the total charge in the device at V_{OC}.

According to all of the above transient measurements, we have shown that the performance of the P3HT:CdSe devices is limited by trapping. There is a higher density of deep traps with decreasing NC size. These deep trap states result in more severe trap-mediated recombination in smaller devices, which is consistent with the decreasing steady-state photocurrent as the NC size decreases. The increasing density of trap states contributes to the increasing difficulty to fill up the traps in the smaller devices.

With the above knowledge in mind, we propose a diagram in Figure 8 describing the density of trap states of CdSe NCs with different sizes. The trap energy is assumed to be constant, and the NC band edge moves toward the vacuum level due to quantum confinement with decreasing size. As a result, the trap depth relative to the band edge increases with decreasing NC size. The density of trap states distribution is shown as exponential, although other shapes are possible.

With this diagram, it becomes clear why the small device has smaller V_{OC}, in spite of its higher LUMO level. In operation, V_{OC} is determined by the quasi-Fermi level splitting between the donor and acceptor, rather than the difference between donor HOMO and acceptor LUMO. The deeper trap states in the small device are detrimental to its V_{OC}, as the quasi-Fermi level is kept in the tail of the trap states and is difficult to raise up to

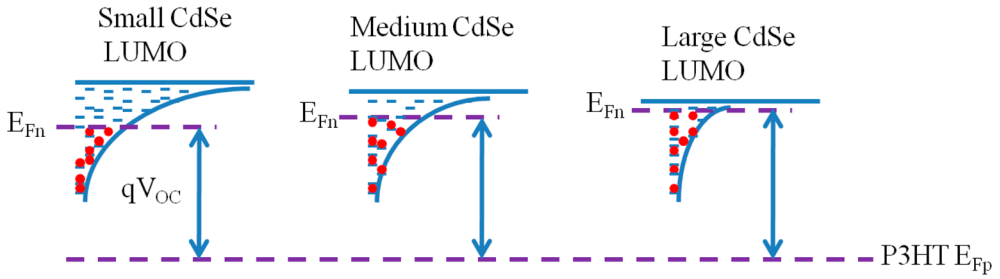

Figure 8. Schematic illustration of the density of trap states changing with CdSe NC size. The effect of the trap distribution on V_{OC} is also illustrated.

the LUMO level. Although the HOMO and LUMO levels provide a first approximation for V_{OC}, the distribution of traps is also a determining factor. Recent publications have noted the effect of the energetic disorder on V_{OC}.[37−42] For example, Garcia-Belmonte *et al.*[38] investigated P3HT blended with two different fullerenes, which share the same LUMO. By performing impedance spectroscopy measurements, the V_{OC} difference between the two blends was attributed to different electron density of states of the two fullerenes. More recently, Blakesley *et al.* also demonstrated that energetic disorder can be responsible for a loss of V_{OC} in BHJ OPVs using numerical device simulations.[42]

CONCLUSIONS

In conclusion, we employed a range of steady-state, quasi-steady-state, and transient measurements to investigate the loss mechanisms in hybrid solar cells. We performed TA measurements on working devices and suggest that the faster decay in the TA kinetics for the small device is due to stronger trap-mediated recombination. Further information on traps is uncovered by photoinduced absorption and transient photocurrent measurements, which confirm that the performance improvement is related to decreasing trapping effects in devices with larger NCs. We conclude that the trap-mediated recombination is responsible for the loss of photogenerated charge carriers in hybrid solar cells. With the information uncovered from the transient photocurrent and absorption measurements, we propose a diagram describing the density of trap states of CdSe NCs with different sizes. With this diagram, we can successfully explain why V_{OC} increases as the NC size increases. Therefore, decreasing the trap density in polymer/nanocrystal blends such as by surface engineering is likely to be an effective approach to improve the efficiency of this class of photovoltaic devices.

METHODS

Nanocrystal Synthesis. CdSe NCs with three different sizes were synthesized using the method by Yu and Peng.[43] Cd precursor was prepared by dissolving CdO powder in oleic acid and 1-octadecene in a flask. Se precursor was prepared separately by dissolving Se powder in trioctylphosphine at 80 °C. When the Cd precursor was heated to 230 °C, Se precursor was quickly injected into the flask. A small aliquot of the reaction solution was frequently taken out to monitor the NC growth using a UV−vis spectrometer. The NC growth slowed around 20 min after Se injection. In order to synthesize even larger NCs, a second injection of Se precursor was required.[44] As soon as the optical absorption spectrum indicated that the target nanocystal size was reached, the reaction was halted. Methanol was added to precipitate the NCs, which were then dissolved in butylamine and stirred overnight in an inert atmosphere for ligand exchange. The butylamine-capped nanodots were recovered by precipitation with methanol. Finally, the nanodots were dissolved in chloroform for device fabrication.

Device Fabrication. PEDOT:PSS layer (40 nm) was spin-coated onto cleaned and plasma-treated ITO substrates, which were then annealed at 150 °C for 30 min under nitrogen atmosphere before being transferred into a glovebox for further fabrication steps. P3HT was dissolved in 1,2,4-trichlorobenzene with a concentration of 30 mg/mL, which was then mixed with CdSe (30 mg/mL in chloroform) to get the blend solution (weight ratio, P3HT:CdSe = 1:9). P3HT:CdSe solution was spin-coated onto the substrates to get 80 ± 5 nm thick films, which were annealed at 150 °C for 30 min in an inert atmosphere. The evaporation of aluminum (100 nm) onto the active layer concludes the fabrication processes and defines the area of the active layer as 4.5 mm^2.

Transient Absorption Measurements. The reflection mode was used to measure the TA signal in a working device, as detailed elsewhere.[20] In short, the pump and probe pulses enter the device through the ITO anode, and the probe signal is collected after being reflected off the Al cathode. The pump beam was adjusted to ensure that the EQE at low pump intensity approached that measured under CW condition. The probe was then aligned to maximize the TA signal, which guarantees maximum overlap of the pump and probe beams.

Transient Photocurrent Measurements. A high-brightness 525 nm green LED was used as the light source for transient photocurrent measurements. The pulse width was 200 μs, with a rise and fall time less than 50 ns. A neutral density filter wheel was used to vary the pulse intensity. The device was connected in series with an Agilent DSO6052A digitizing oscilloscope (input impedance 50 Ω). For background-dependent transient photocurrent measurements, the background light was provided by a white high-brightness LED.

It is important to ensure that the dynamics in transient photocurrent measurements are not limited by the RC time constant of the circuit. From the 50 Ω external resistance, R, and the geometrical capacitance of ∼4 nF (assuming an average dielectric constant of ∼7), we find that RC is less than 200 ns, much shorter than the time constants we observe.

Transient Photovoltage Measurements. Transient photovoltage measurements were performed using a similar setup as for the photocurrent measurements with the device connected to the oscilloscope (1 MΩ input impedance). The light intensity of

the pulsed light was kept sufficiently low such that the voltage perturbation was always less than 5% of the open-circuit voltage for the given background illumination intensity. Background illumination was provided by a white high-brightness LED.

Conflict of Interest: The authors declare no competing financial interest.

Acknowledgment. We are grateful to the Cambridge Overseas Trust, the China Scholarship Council, and the Engineering and Physical Sciences Research Council, U.K (Grant Number EP/G060738/1) for financial support.

REFERENCES AND NOTES

1. Greenham, N. C.; Peng, X.; Alivisatos, A. P. Charge Separation and Transport in Conjugated-Polymer/Semiconductor-Nanocrystal Composites Studied by Photoluminescence Quenching and Photoconductivity. *Phys. Rev. B* **1996**, *54*, 17628–17637.
2. Huynh, W. U.; Peng, X.; Alivisatos, A. P. CdSe Nanocrystal Rods/Poly(3-hexylthiophene) Composite Photovoltaic Devices. *Adv. Mater.* **1999**, *11*, 923–927.
3. Sun, B.; Marx, E.; Greenham, N. C. Photovoltaic Devices Using Blends of Branched CdSe Nanoparticles and Conjugated Polymers. *Nano Lett.* **2003**, *3*, 961–963.
4. Dayal, S.; Kopidakis, N.; Olson, D. C.; Ginley, D. S.; Rumbles, G. Photovoltaic Devices with a Low Band Gap Polymer and CdSe Nanostructures Exceeding 3% Efficiency. *Nano Lett.* **2010**, *10*, 239–242.
5. Gao, F.; Ren, S.; Wang, J. The Renaissance of Hybrid Solar Cells: Progresses, Challenges, and Perspectives. *Energy Environ. Sci.* **2013**, *6*, 2020–2040.
6. Ren, S.; Chang, L.-Y.; Lim, S.-K.; Zhao, J.; Smith, M.; Zhao, N.; Bulović, V.; Bawendi, M.; Gradečak, S. Inorganic–Organic Hybrid Solar Cell: Bridging Quantum Dots to Conjugated Polymer Nanowires. *Nano Lett.* **2011**, *11*, 3998–4002.
7. Dayal, S.; Reese, M. O.; Ferguson, A. J.; Ginley, D. S.; Rumbles, G.; Kopidakis, N. The Effect of Nanoparticle Shape on the Photocarrier Dynamics and Photovoltaic Device Performance of Poly(3-hexylthiophene):CdSe Nanoparticle Bulk Heterojunction Solar Cells. *Adv. Funct. Mater.* **2010**, *20*, 2629–2635.
8. Yu, W. W.; Qu, L.; Guo, W.; Peng, X. Experimental Determination of the Extinction Coefficient of CdTe, CdSe, and CdS Nanocrystals. *Chem. Mater.* **2003**, *15*, 2854–2860.
9. Cheyns, D.; Poortmans, J.; Heremans, P.; Deibel, C.; Verlaak, S.; Rand, B. P.; Genoe, J. Analytical Model for the Open-Circuit Voltage and Its Associated Resistance in Organic Planar Heterojunction Solar Cells. *Phys. Rev. B* **2008**, *77*, 165332.
10. Cowan, S. R.; Roy, A.; Heeger, A. J. Recombination in Polymer-Fullerene Bulk Heterojunction Solar Cells. *Phys. Rev. B* **2010**, *82*, 245207.
11. Tyagi, P.; Cooney, R. R.; Sewall, S. L.; Sagar, D. M.; Saari, J. I.; Kambhampati, P. Controlling Piezoelectric Response in Semiconductor Quantum Dots via Impulsive Charge Localization. *Nano Lett.* **2010**, *10*, 3062–3067.
12. Kambhampati, P. Hot Exciton Relaxation Dynamics in Semiconductor Quantum Dots: Radiationless Transitions on the Nanoscale. *J. Phys. Chem. C* **2011**, *115*, 22089–22109.
13. Kambhampati, P. Unraveling the Structure and Dynamics of Excitons in Semiconductor Quantum Dots. *Acc. Chem. Res.* **2011**, *44*, 1–13.
14. Hwang, I.-W.; Moses, D.; Heeger, A. J. Photoinduced Carrier Generation in P3HT/PCBM Bulk Heterojunction Materials. *J. Phys. Chem. C* **2008**, *112*, 4350–4354.
15. Hodgkiss, J. M.; Campbell, A. R.; Marsh, R. A.; Rao, A.; Albert-Seifried, S.; Friend, R. H. Subnanosecond Geminate Charge Recombination in Polymer–Polymer Photovoltaic Devices. *Phys. Rev. Lett.* **2010**, *104*, 177701.
16. Albero, J.; Martínez-Ferrero, E.; Ajuria, J.; Waldauf, C.; Pacios, R.; Palomares, E. Photo-induced Electron Recombination Dynamics in CdSe/P3HT Hybrid Heterojunctions. *Phys. Chem. Chem. Phys.* **2009**, *11*, 9644–9647.
17. Albero, J.; Zhou, Y.; Eck, M.; Rauscher, F.; Niyamakom, P.; Dumsch, I.; Allard, S.; Scherf, U.; Krüger, M.; Palomares, E. Photo-induced Charge Recombination Kinetics in Low Bandgap PCPDTBT Polymer:CdSe Quantum Dot Bulk Heterojunction Solar Cells. *Chem. Sci.* **2011**, *2*, 2396–2401.
18. Jamieson, F. C.; Agostinelli, T.; Azimi, H.; Nelson, J.; Durrant, J. R. Field-Independent Charge Photogeneration in PCPDTBT/$PC_{70}BM$ Solar Cells. *J. Phys. Chem. Lett.* **2010**, *1*, 3306–3310.
19. Friend, R. H.; Phillips, M.; Rao, A.; Wilson, M. W. B.; Li, Z.; McNeill, C. R. Excitons and Charges at Organic Semiconductor Heterojunctions. *Faraday Discuss.* **2012**, *155*, 339–348.
20. Marsh, R. A.; Hodgkiss, J. M.; Friend, R. H. Direct Measurement of Electric Field-Assisted Charge Separation in Polymer:Fullerene Photovoltaic Diodes. *Adv. Mater.* **2010**, *22*, 3672–3676.
21. Österbacka, R.; An, C. P.; Jiang, X. M.; Vardeny, Z. V. Two-Dimensional Electronic Excitations in Self-Assembled Conjugated Polymer Nanocrystals. *Science* **2000**, *287*, 839–842.
22. Ohkita, H.; Cook, S.; Astuti, Y.; Duffy, W.; Tierney, S.; Zhang, W.; Heeney, M.; McCulloch, I.; Nelson, J.; Bradley, D. D. C.; *et al.* Charge Carrier Formation in Polythiophene/Fullerene Blend Films Studied by Transient Absorption Spectroscopy. *J. Am. Chem. Soc.* **2008**, *130*, 3030–3042.
23. De, S.; Pascher, T.; Maiti, M.; Jespersen, K. G.; Kesti, T.; Zhang, F.; Inganäs, O.; Yartsev, A.; Sundström, V. Geminate Charge Recombination in Alternating Polyfluorene Copolymer/Fullerene Blends. *J. Am. Chem. Soc.* **2007**, *129*, 8466–8472.
24. Ginger, D.; Greenham, N. Photoinduced Electron Transfer from Conjugated Polymers to CdSe Nanocrystals. *Phys. Rev. B* **1999**, *59*, 10622–10629.
25. Cole, K. S.; Cole, R. H. Dispersion and Absorption in Dielectrics I. Alternating Current Characteristics. *J. Chem. Phys.* **1941**, *9*, 341.
26. Wang, P.; Abrusci, A.; Wong, H. M. P.; Svensson, M.; Andersson, M. R.; Greenham, N. C. Photoinduced Charge Transfer and Efficient Solar Energy Conversion in a Blend of a Red Polyfluorene Copolymer with CdSe Nanoparticles. *Nano Lett.* **2006**, *6*, 1789–1793.
27. Heinemann, M. D.; von Maydell, K.; Zutz, F.; Kolny-Olesiak, J.; Borchert, H.; Riedel, I.; Parisi, J. Photo-induced Charge Transfer and Relaxation of Persistent Charge Carriers in Polymer/Nanocrystal Composites for Applications in Hybrid Solar Cells. *Adv. Funct. Mater.* **2009**, *19*, 3788–3795.
28. Li, Z.; Gao, F.; Greenham, N. C.; McNeill, C. R. Comparison of the Operation of Polymer/Fullerene, Polymer/Polymer, and Polymer/Nanocrystal Solar Cells: A Transient Photocurrent and Photovoltage Study. *Adv. Funct. Mater.* **2011**, *21*, 1419–1431.
29. Li, Z.; McNeill, C. R. Transient Photocurrent Measurements of PCDTBT:$PC_{70}BM$ and PCPDTBT:$PC_{70}BM$ Solar Cells: Evidence for Charge Trapping in Efficient Polymer/Fullerene Blends. *J. Appl. Phys.* **2011**, *109*, 074513.
30. McNeill, C. R.; Hwang, I.; Greenham, N. C. Photocurrent Transients in All-Polymer Solar Cells: Trapping and Detrapping Effects. *J. Appl. Phys.* **2009**, *106*, 024507.
31. Hwang, I.; McNeill, C. R.; Greenham, N. C. Drift-Diffusion Modeling of Photocurrent Transients in Bulk Heterojunction Solar Cells. *J. Appl. Phys.* **2009**, *106*, 094506.
32. Gao, F.; Wang, J.; Blakesley, J. C.; Hwang, I.; Li, Z.; Greenham, N. C. Quantifying Loss Mechanisms in Polymer:Fullerene Photovoltaic Devices. *Adv. Energy Mater.* **2012**, *2*, 956–961.
33. Mooney, J.; Krause, M. M.; Saari, J. I.; Kambhampati, P. Challenge to the Deep-Trap Model of the Surface in Semiconductor Nanocrystals. *Phys. Rev. B* **2013**, *87*, 081201.
34. Tyagi, P.; Kambhampati, P. False Multiple Exciton Recombination and Multiple Exciton Generation Signals in Semiconductor Quantum Dots Arise from Surface Charge Trapping. *J. Chem. Phys.* **2011**, *134*, 094706.
35. Sewall, S. L.; Cooney, R. R.; Anderson, K. E. H.; Dias, E. A.; Sagar, D. M.; Kambhampati, P. State-Resolved Studies of Biexcitons and Surface Trapping Dynamics in Semiconductor Quantum Dots. *J. Chem. Phys.* **2008**, *129*, 084701.

36. O'Regan, B. C.; Scully, S.; Mayer, A. C.; Palomares, E.; Durrant, J. The Effect of Al_2O_3 Barrier Layers in TiO_2/Dye/CuSCN Photovoltaic Cells Explored by Recombination and DOS Characterization Using Transient Photovoltage Measurements. *J. Phys. Chem. B* **2005**, *109*, 4616–4623.
37. Blakesley, J. C.; Greenham, N. C. Charge Transfer at Polymer-Electrode Interfaces: The Effect of Energetic Disorder and Thermal Injection on Band Bending and Open-Circuit Voltage. *J. Appl. Phys.* **2009**, *106*, 034507.
38. Garcia-Belmonte, G.; Boix, P. P.; Bisquert, J.; Lenes, M.; Bolink, H. J.; La Rosa, A.; Filippone, S.; Martín, N. Influence of the Intermediate Density-of-States Occupancy on Open-Circuit Voltage of Bulk Heterojunction Solar Cells with Different Fullerene Acceptors. *J. Phys. Chem. Lett.* **2010**, *1*, 2566–2571.
39. Garcia-Belmonte, G.; Bisquert, J. Open-Circuit Voltage Limit Caused by Recombination through Tail States in Bulk Heterojunction Polymer-Fullerene Solar Cells. *Appl. Phys. Lett.* **2010**, *96*, 113301.
40. Garcia-Belmonte, G.; Boix, P. P.; Bisquert, J.; Sessolo, M.; Bolink, H. J. Simultaneous Determination of Carrier Lifetime and Electron Density-of-States in P3HT:PCBM Organic Solar Cells under Illumination by Impedance Spectroscopy. *Sol. Energy Mater. Sol. Cells* **2010**, *94*, 366–375.
41. Nayak, P. K.; Bisquert, J.; Cahen, D. Assessing Possibilities and Limits for Solar Cells. *Adv. Mater.* **2011**, *23*, 2870–2876.
42. Blakesley, J. C.; Neher, D. Relationship between Energetic Disorder and Open-Circuit Voltage in Bulk Heterojunction Organic Solar Cells. *Phys. Rev. B* **2011**, *84*, 075210.
43. Yu, W. W.; Peng, X. Formation of High-Quality CdS and Other II−VI Semiconductor Nanocrystals in Noncoordinating Solvents: Tunable Reactivity of Monomers. *Angew. Chem., Int. Ed.* **2002**, *41*, 2368–2371.
44. Peng, X.; Wickham, J.; Alivisatos, A. P. Kinetics of II−VI and III−V Colloidal Semiconductor Nanocrystal Growth: "Focusing" of Size Distributions. *J. Am. Chem. Soc.* **1998**, *120*, 5343–5344.